

# Femtosecond spin-state switching dynamics of spin-crossover molecules condensed in thin films

Lea Kämmerer<sup>1†</sup>, Gérald Kämmerer<sup>1†</sup>, Manuel Gruber<sup>1\*</sup>, Jan Grunwald<sup>2</sup>, Tobias Lojewski<sup>1</sup>, Laurent Mercadier<sup>3</sup>, Loïc Le Guyader<sup>3</sup>, Robert Carley<sup>3</sup>, Camille Carinan<sup>3</sup>, Natalia Gerasimova<sup>3</sup>, David Hickin<sup>3</sup>, Benjamin E. Van Kuiken<sup>3</sup>, Giuseppe Mercurio<sup>3</sup>, Martin Teichmann<sup>3</sup>, Senthil Kumar Kuppusamy<sup>4</sup>, Andreas Scherz<sup>3</sup>, Mario Ruben<sup>4,5</sup>, Klaus Sokolowski-Tinten<sup>1</sup>, Andrea Eschenlohr<sup>1</sup>, Katharina Ollefs<sup>1</sup>, Carolin Schmitz-Antoniak<sup>6</sup>, Felix Tuzek<sup>2</sup>, Peter Kratzer<sup>1</sup>, Uwe Bovensiepen<sup>1</sup>, Heiko Wende<sup>1</sup>

<sup>1</sup> Faculty of Physics and Center for Nanointegration Duisburg-Essen (CENIDE), University of Duisburg-Essen; Duisburg, 47048, Germany.

<sup>2</sup> Institute for Inorganic Chemistry, Christian-Albrechts-University; Kiel, 24098, Germany.

<sup>3</sup> European XFEL; Schenefeld, 22869, Germany.

<sup>4</sup> Institute for Quantum Materials and Technologies (IQMT), Karlsruhe Institute for Technology (KIT); Eggstein-Leopoldshafen, 76344, Germany.

<sup>5</sup> Centre Européen de Sciences Quantiques (CESQ), Institut de Science et d'Ingénierie Supramoléculaires (ISIS); Strasbourg Cedex, 67083, France.

<sup>6</sup> Faculty of Engineering and Natural Sciences, Technical University of Applied Science Wildau; Wildau, 15745, Germany.

†These authors contributed equally to this work

Corresponding author: [manuel.gruber@uni-due.de](mailto:manuel.gruber@uni-due.de)

## Abstract

The photoinduced switching of Fe(II)-based spin-crossover complexes from singlet to quintet takes place at ultrafast time scales. This a priori spin-forbidden transition triggered numerous time-resolved experiments of solvated samples to elucidate the mechanism at play. The involved intermediate states remain uncertain. We apply ultrafast x-ray spectroscopy in molecular films as a method sensitive to spin, electronic, and nuclear degrees of freedom. Combining the progress in molecule synthesis and film growth with the opportunities at x-ray free-electron lasers, we analyze the transient evolution of the Fe  $L_3$  fine structure at room temperature. Our measurements and calculations indicate the involvement of an Fe triplet intermediate state. The high-spin state saturates at half of the available molecules, limited by molecule-molecule interaction within the film.

## Introduction

The electronic configuration and the associated spin state of an Fe(II) ion in an octahedral symmetry is controlled by the strength of the ligand field, which splits the  $3d$  electronic states into  $e_g$  and  $t_{2g}$  orbitals and scales with the average length of the coordination bonds. This phenomenon is illustrated in Fig. 1. For spin-crossover complexes, the transition between the two stable states – a singlet ( $S = 0$ ) low-spin and a quintet ( $S = 2$ ) high-spin state – can be induced by various stimuli including temperature and light absorption (1). Such molecular compounds, in particular those that can be operated at room temperature up to terahertz bandwidth using photoexcitation, have prospects for technological applications but require cooperative effects in condensed films rather than solvated samples of diluted molecules.

The photoinduced dynamics of complexes in solutions have been studied using pump-probe experiments employing optical (2–5), hard (6–9), and soft x-ray (10, 11) probes along with *ab initio* calculations (12, 13). The broadly accepted microscopic mechanism upon optical excitation proceeds on femtosecond timescales. It involves the population of a metal-to-ligand-charge-transfer (MLCT) singlet state starting from the low-spin ground state, followed by an ultrafast relaxation along the multidimensional Fe-N nuclear coordinate to the  $S = 2$  quintet *via* intersystem crossing (12, 13). The details of the relaxation pathway are actively investigated, for instance, regarding the nature of the intermediate state: a triplet  $^3\text{MLCT}$  or a metal-centered triplet  $^3\text{T}_2$  state. Recent time-resolved spectroscopic measurements at the Fe  $K$  and  $M$  edges favor a metal-centered intermediate state (7, 14, 15).

The fine structure analyzed in x-ray absorption spectroscopy close to the Fe  $L_3$  absorption edge is largely sensitive to the electronic occupation of the  $3d$  orbitals, and is particularly informative about the correlated structural, spin, and electronic degrees of freedom upon the spin crossover transition. However, as the soft x-rays are absorbed by the solvent, the element-specific experiments were almost exclusively performed at the Fe  $K$  edge (6, 9, 15), or resorting to a liquid film of solvated molecules (10, 11). With the availability of x-ray free electron laser (XFEL) sources, a new quality of femtosecond soft x-ray absorption spectroscopy was demonstrated recently (9, 16–18), including the sensitivity to intermediate states in chemical reactions (19).

The synthesis of sublimable SCO compounds and the elaboration of high-quality thin films significantly progressed over the last years (20–22). Homogeneous films can nowadays be prepared with molecules presumably withstanding high x-ray and optical fluences. Such samples allow investigating the impact of the molecule-molecule interactions on the spin-switching dynamics. The ultrafast optical response of such films indicates ultrafast photo-switching, while evidencing additional thermally induced dynamics in films with thickness above 50 nm (23), as previously observed on single crystals (4, 24). Such samples are also investigated at the Fe  $M$  edge with complementary table-top methods (14), which can presently reach the Fe  $L$  edge with picosecond time resolution (25).

Here, we reveal the room-temperature switching mechanism of an ultrathin film of Fe(pypypyr) $_2$  [pypypyr = bipyridyl pyrrolide] (see Fig. 1) sublimated on Si $_3$ N $_4$ . Details on sample preparation and characterization are provided in the supplementary materials. The transient evolution of the absorption fine structure at the Fe  $L_3$  edge from the singlet to quintet state is triggered by optical pumping and analyzed with 80 fs time resolution. The results showcase the transient population of a metal-centered triplet intermediate state in the switching

dynamics. By increasing the density of optically excited molecules in the material, we identify a limit of  $\sim 40\%$  of switched molecules, which is rationalized primarily by the large molecular distortion that leads to local stress. For switching a large fraction of molecules such stress must be relaxed locally, presumably by unswitched molecules adjacent to switched ones.

## Results and discussion

We used the Spectroscopy and Coherent Scattering instrument at the European XFEL, which provides a shot-to-shot normalization scheme with high signal-to-noise ratio in the x-ray spectra (Fig. 2A) (17, 18, 26). The x-ray absorption spectra were measured in transmission geometry in a pump-probe configuration by sweeping the photon energy of ultrashort x-ray pulses [full width at half maximum (FWHM) of 30-60 fs] synchronized with an ultrashort pump pulse at 3.1 eV photon energy and a FWHM pulse duration of 50 fs. For further technical details, see supplementary materials and Ref. (17). The chosen photon energy of the optical pump pulse induces a resonant excitation from the low-spin ground state to a MLCT state, in turn relaxing to the high-spin state. The x-ray pulse probes the transient state after a pump probe time delay  $\Delta t$ , see Fig. 2A.

Resonant absorption at the Fe  $L_3$  absorption edge ( $2p_{3/2} \rightarrow 3d$ ) probes the unoccupied electronic states of the  $t_{2g}$  and  $e_g$  orbitals (Fig. 2B). This method is well-established to quantify the fractions of low- and high-spin molecules (21, 22, 27, 28). In the absence of pumping, the x-ray absorption spectrum exhibits a main peak at 708.9 eV indicating a low-spin state of the molecules at room temperature. A pumped spectrum at  $\Delta t=3$  ps exhibits an increase and decrease in x-ray absorption at 707.1 eV and 708.9 eV, respectively, which is shown in Fig. 2C in comparison to a spectrum obtained without pumping. The difference of the pumped and unpumped spectra is shown in the lower panel of Fig. 2C as the pump-induced change which is clearly identified and reaches 20%. This value represents a change of population from the low to the high spin state (28).

Fig. 3A shows the evolution of the x-ray absorption at 707.1 and 708.9 eV as a function of pump probe time delay. While the absorption changes by  $\sim 15\%$  for both delay sweeps, the saturation is reached faster within 0.3 ps at 708.9 eV than at 707.1 eV, where reaching saturation takes 0.5 ps. The difference between the two transients is significant for  $0 < \Delta t < 0.5$  ps as depicted in the bottom panel of Fig. 2C, which indicates the transient population of an intermediate state. We emphasize that the transition from the low- to the high-spin configuration involves an electronically excited state in combination with a change of nuclear coordinates.

We simulate x-ray absorption spectra using atomic multiplet and ligand-field theory (29, 30) (see supplementary materials). Assuming the ligand field of the low-spin state,  $10 Dq = 2.6$  eV as inferred from our density functional theory (DFT) calculations, we obtain the spectra for the electronic excitations corresponding to the ground state singlet  $^1A_1$ , the intermediate Fe-based triplet  $^3T_2$ , and the high-spin quintet  $^5T_2$  before N displacement has occurred, see Fig. 3B. Here,  $^3T_2$  and  $^5T_2$  are distinguished by different energies of pre-edge features below 708 eV and different contributions post-edge above 709.5 eV. This approach nicely reproduces the measured low-spin spectrum before excitation, compare the blue lines in Fig. 3B,C. We acquired transient x-ray absorption spectra at the early instants of the dynamics at  $\Delta t < 0.25$  ps shown in Fig. 3C and in the supplementary materials. Compared to spectra recorded before pumping and at  $\Delta t=3$  ps, a small but significant increase in x-ray absorption is observed pre-

edge at 706.3 eV and, although weaker, post-edge at 710 eV. The x-ray spectrum measured at 195 fs, see Fig. 3C, reflects a transient population of the Fe-centered state  $^3T_2$  with the nuclear configuration of the low-spin state in addition to molecules that have already switched to the high-spin state as well as low-spin molecules. According to the calculations, the occupation of a transient  $^5T_2$  state (also with the nuclear configuration of the low-spin state) should lead to an increased x-ray absorption at 705.5 eV, which is not observed in the experimental spectrum at 195 fs and thus discarded as an intermediate state.

Quantum chemistry (12, 13) and time-dependent DFT (31) calculations have been successfully employed in the past to describe spin-crossover complexes. Here, we use both static and time-dependent DFT, see supplementary materials, since this allows us to calculate potential energy surfaces of different electronic states including the ligand orbitals. The atomic configuration in the intermediate  $S = 1$  state is obtained by performing geometry optimization in a spin-restricted DFT calculation. Subsequent linear-response TD-DFT calculations allow us to address electronic excitations not only in the Fe ion, but in the whole molecule. The determined energies include all electrons with their interactions. Fig. 4 shows the obtained potential energy surfaces of the singlet ground state  $^1A_1$  (blue), the singlet  $^1MLCT$  (gray area), triplet states located at the ligands (black), as well as the metal centered triplet  $^3T_2$  (brown) and quintet  $^5T_2$  (red) as a function of the nuclear coordinate. The latter is represented as the N displacement measured from the intermediate  $S = 1$  state towards the  $S = 0$  initial state (negative) and towards the  $S = 2$  final state (positive values). The optical pump at 3.1 eV photon energy induces a resonant transition from the low-spin configuration to the  $^1MLCT$  manifold following the dipole selection rule. The transition to the final quintet state necessitates the evolution over an intermediate triplet state, which is provided by the ligand-based triplets and/or the metal-centered  $^3T_2$  state. Both scenarios lead to different possible relaxation pathways illustrated in Fig. 4. (i) Transfer from  $^1MLCT$  to ligand-based triplets, followed by transfer to the quintet potential energy surface (top curved arrow) and relaxation along the red arrow to the high-spin configuration. (ii) Electron relaxation out of  $^1MLCT$  into vibrational excited states of  $^3T_2$  (vertical solid and dashed black arrows) followed by N displacement to  $^5T_2$  (horizontal arrow). (iii) Relaxation at the low (or intermediate) spin nuclear configuration by subsequent steps (curved arrows) to vibrationally excited  $^3T_2$  and N displacement to reach the high-spin state (horizontal arrow).

Having identified the contribution of the Fe-based triplet state by x-ray spectroscopy we propose that the population of the optically excited intermediate state, see Fig. 3A (bottom), represents a nuclear wave packet residing initially in a triplet state. Pathways (i-iii) agree with this proposal. We discard (i) in the further discussion because it does not involve  $^3T_2$ . Our experimental data does not allow to distinguish between (ii) and (iii). In addition, theoretical investigations (32) have shown the strong mixing of electronic, nuclear, and spin degrees of freedom suggesting more complex relaxation paths and both could contribute. The different time evolution of the two x-ray absorption features shown in Fig. 3A can be reproduced well using a rate equation model assuming a single  $^3T_2$  intermediate state with a finite relaxation time, see supplementary materials. It should be noted that the involvement of a ligand-centered triplet  $^3MLCT$  state, prior to the  $^3T_2$  population, cannot be excluded. Our data indicate that the lifetime of the  $^3MLCT$  state, if populated, is significantly shorter than that of the  $^3T_2$  state. In this molecular material, the nuclear relaxation from the  $^3T_2$  state to the high-spin geometry

occurs extremely fast, within 70 fs according to our molecular dynamics calculations (see supplementary materials).

An essential difference between molecular films and individual molecules in solution is the presence of molecule-molecule interactions in the condensed phase. It might have considerable impact on the switching process that is essential in potential future applications of such films. Since the pump absorption determines the number of optically excited molecules, analysis of the switching yield as a function of pump fluence may provide insight into the interaction of excited molecules among each other in the molecular film. Fig. 5 shows the normalized pump-induced change as a function of incident pump fluence up to 15 mJ/cm<sup>2</sup> at a fixed pump-probe delay of 3 ps. The absolute values of the pump-induced changes of the corresponding fine structure x-ray energies, which were introduced in Fig. 2C, increase linearly with the fluence up to approximately 5 mJ/cm<sup>2</sup>. This behavior suggests an absence of interactions between excited molecules in this regime. For fluences of 3 to 6 mJ/cm<sup>2</sup> the changes saturate for both x-ray energies. As detailed in the supplementary materials, a fluence of 13 mJ/cm<sup>2</sup> corresponds in the investigated films to approximately one absorbed pump photon per spin crossover molecule. We estimate from the fluence at which the saturation is reached in Fig. 5 that 30 to 50% of the molecules in the film are transiently excited to the high-spin state. This implies that although sufficient pump photons reach the film, a large fraction of the molecules does not participate in the switching process. Such a behavior was reported earlier for static measurements for the present molecule (28) as well as other complexes (33, 34), and rationalized by steric-repulsion considerations. For a fraction of the molecules, the high-spin state is unfavorable due to the interaction with neighboring molecules. The unfavorable high-spin configuration may either lead to a fast relaxation to the low-spin state or completely prevent the switching. Although stationary experiments cannot distinguish between these two scenarios, our data with ultrafast time resolution strengthen the second scenario.

With our results we showcase opportunities provided by ultrafast x-ray spectroscopy at modern light sources like x-ray free electron lasers for the field of spin crossover phenomena in molecular films. We identified a metal-centered triplet state as an intermediate electronic state in the low- to high-spin transition and propose a switching yield limit imposed by the involved intra- and intermolecular restructuring. Thereby, we highlight the sensitivity of this spectroscopy to the spin character of the electronically excited state correlated with the nuclear coordinate which is fundamental to the low- to high-spin transition. Considering different complexes, the relative importance of the <sup>3</sup>T<sub>2</sub> and <sup>3</sup>MLCT states is expected to depend on the actual strength of the ligand field (35). In the future, the opportunities opened here by our work to exploit the connection of intramolecular parameters like the ligand field with structural parameters of intermolecular arrangement in condensed films might lead to identification of microscopic interaction principles in such films. Hence, combining structure-specific interactions resulting from the molecular arrangement in thin films with intra-molecular, chemically controlled characteristics, such as the ligand field strength, may open up further opportunities for material design.

## Materials and Methods

The description of the Materials and Methods is described in the Supplementary Materials.

## References

1. P. Gütllich, Y. Garcia, H. A. Goodwin, Spin crossover phenomena in Fe (II) complexes. *Chem. Soc. Rev.* **29**, 419–427 (2000).
2. W. Gawelda, A. Cannizzo, V.-T. Pham, F. Van Mourik, C. Bressler, M. Chergui, Ultrafast Nonadiabatic Dynamics of  $[\text{Fe}^{\text{II}}(\text{bpy})_3]^{2+}$  in Solution. *J. Am. Chem. Soc.* **129**, 8199–8206 (2007).
3. A. L. Smeigh, M. Creelman, R. A. Mathies, J. K. McCusker, Femtosecond Time-Resolved Optical and Raman Spectroscopy of Photoinduced Spin Crossover: Temporal Resolution of Low-to-High Spin Optical Switching. *J. Am. Chem. Soc.* **130**, 14105–14107 (2008).
4. M. Lorenc, J. Hébert, N. Moisan, E. Trzop, M. Servol, M. Buron-Le Cointe, H. Cailleau, M. L. Boillot, E. Pontecorvo, M. Wulff, S. Koshihara, E. Collet, Successive Dynamical Steps of Photoinduced Switching of a Molecular Fe(III) Spin-Crossover Material by Time-Resolved X-Ray Diffraction. *Phys. Rev. Lett.* **103**, 028301 (2009).
5. M. M. N. Wolf, R. Groß, C. Schumann, J. A. Wolny, V. Schünemann, A. Døssing, H. Paulsen, J. J. McGarvey, R. Diller, Sub-picosecond time resolved infrared spectroscopy of high-spin state formation in Fe(ii) spin crossover complexes. *Phys. Chem. Chem. Phys.* **10**, 4264 (2008).
6. C. Bressler, C. Milne, V.-T. Pham, A. ElNahas, R. M. van der Veen, W. Gawelda, S. Johnson, P. Beaud, D. Grolimund, M. Kaiser, C. N. Borca, G. Ingold, R. Abela, M. Chergui, Femtosecond XANES Study of the Light-Induced Spin Crossover Dynamics in an Iron(II) Complex. *Science* **323**, 489–492 (2009).
7. W. Zhang, R. Alonso-Mori, U. Bergmann, C. Bressler, M. Chollet, A. Galler, W. Gawelda, R. G. Hadt, R. W. Hartsock, T. Kroll, K. S. Kjær, K. Kubiček, H. T. Lemke, H. W. Liang, D. A. Meyer, M. M. Nielsen, C. Purser, J. S. Robinson, E. I. Solomon, Z. Sun, D. Sokaras, T. B. Van Driel, G. Vankó, T.-C. Weng, D. Zhu, K. J. Gaffney, Tracking excited-state charge and spin dynamics in iron coordination complexes. *Nature* **509**, 345–348 (2014).
8. G. Azzolina, E. Collet, C. Mariette, M. Cammarata, E. Trzop, M. Sander, M. Levantino, K. Nakagawa, H. Tokoro, S. Ohkoshi, R. Bertoni, Single Laser Shot Photoinduced Phase Transition of Rubidium Manganese Hexacyanoferrate Investigated by X-ray Diffraction. *Eur J Inorg Chem* **2019**, 3142–3147 (2019).
9. H. T. Lemke, K. S. Kjær, R. Hartsock, T. B. Van Driel, M. Chollet, J. M. Glowina, S. Song, D. Zhu, E. Pace, S. F. Matar, M. M. Nielsen, M. Benfatto, K. J. Gaffney, E. Collet, M. Cammarata, Coherent structural trapping through wave packet dispersion during photoinduced spin state switching. *Nat Commun* **8**, 15342 (2017).
10. N. Huse, H. Cho, K. Hong, L. Jamula, F. M. F. de Groot, T. K. Kim, J. K. McCusker, R. W. Schoenlein, Femtosecond Soft X-ray Spectroscopy of Solvated Transition-Metal Complexes: Deciphering the Interplay of Electronic and Structural Dynamics. *J. Phys. Chem. Lett.* **2**, 880–884 (2011).

11. N. Huse, T. K. Kim, L. Jamula, J. K. McCusker, F. M. F. de Groot, R. W. Schoenlein, Photo-Induced Spin-State Conversion in Solvated Transition Metal Complexes Probed via Time-Resolved Soft X-ray Spectroscopy. *J. Am. Chem. Soc.* **132**, 6809–6816 (2010).
12. C. de Graaf, C. Sousa, Study of the Light-Induced Spin Crossover Process of the  $[\text{Fe}^{\text{II}}(\text{bpy})_3]^{2+}$  Complex. *Chem. Eur. J.* **16**, 4550–4556 (2010).
13. C. Sousa, C. de Graaf, A. Rudavskiy, R. Broer, J. Tatchen, M. Etinski, C. M. Marian, Ultrafast Deactivation Mechanism of the Excited Singlet in the Light-Induced Spin Crossover of  $[\text{Fe}(\text{2,2'}$ -bipyridine) $3]^{2+}$ . *Chem. Eur. J.* **19**, 17541–17551 (2013).
14. K. Zhang, R. Ash, G. S. Girolami, J. Vura-Weis, Tracking the Metal-Centered Triplet in Photoinduced Spin Crossover of  $\text{Fe}(\text{phen})_3^{2+}$  with Tabletop Femtosecond M-Edge X-ray Absorption Near-Edge Structure Spectroscopy. *J. Am. Chem. Soc.* **141**, 17180–17188 (2019).
15. K. S. Kjær, T. B. Van Driel, T. C. B. Harlang, K. Kunnus, E. Biasin, K. Ledbetter, R. W. Hartsock, M. E. Reinhard, S. Koroidov, L. Li, M. G. Laursen, F. B. Hansen, P. Vester, M. Christensen, K. Haldrup, M. M. Nielsen, A. O. Dohn, M. I. Pápai, K. B. Møller, P. Chabera, Y. Liu, H. Tatsuno, C. Timm, M. Jarenmark, J. Uhlig, V. Sundstöm, K. Wärnmark, P. Persson, Z. Németh, D. S. Szemes, É. Bajnóczi, G. Vankó, R. Alonso-Mori, J. M. Glowina, S. Nelson, M. Sikorski, D. Sokaras, S. E. Canton, H. T. Lemke, K. J. Gaffney, Finding intersections between electronic excited state potential energy surfaces with simultaneous ultrafast X-ray scattering and spectroscopy. *Chem. Sci.* **10**, 5749–5760 (2019).
16. D. R. Baykusheva, H. Jang, A. A. Husain, S. Lee, S. F. R. TenHuisen, P. Zhou, S. Park, H. Kim, J.-K. Kim, H.-D. Kim, M. Kim, S.-Y. Park, P. Abbamonte, B. J. Kim, G. D. Gu, Y. Wang, M. Mitrano, Ultrafast Renormalization of the On-Site Coulomb Repulsion in a Cuprate Superconductor. *Phys. Rev. X* **12**, 011013 (2022).
17. L. Le Guyader, A. Eschenlohr, M. Beye, W. Schlotter, F. Döring, C. Carinan, D. Hickin, N. Agarwal, C. Boeglin, U. Bovensiepen, J. Buck, R. Carley, A. Castoldi, A. D'Elia, J.-T. Delitz, W. Ehsan, R. Engel, F. Erdinger, H. Fangohr, P. Fischer, C. Fiorini, A. Föhlisch, L. Gelisio, M. Gensch, N. Gerasimova, R. Gort, K. Hansen, S. Hauf, M. Izquierdo, E. Jal, E. Kamil, L. Kämmerer, S. Karabekyan, T. Kluyver, T. Laarmann, T. Lojewski, D. Lomidze, S. Maffessanti, T. Mamyrbayev, A. Marcelli, L. Mercadier, G. Mercurio, P. S. Miedema, K. Ollefs, K. Rossnagel, B. Rösner, N. Rothenbach, A. Samartsev, J. Schlappa, K. Setoodehnia, G. Sorin Chiuzbaian, C. Stamm, F. Stellato, S. Techert, M. Teichmann, M. Turcato, B. Van Kuiken, H. Wende, A. Yaroslavtsev, J. Zhu, S. Molodtsov, C. David, M. Porro, A. Scherz, Photon-shot-noise-limited transient absorption soft X-ray spectroscopy at the European XFEL. *J Synchrotron Rad* **30**, 284–300 (2023).
18. T. Lojewski, M. F. Elhanoty, L. Le Guyader, O. Grånäs, N. Agarwal, C. Boeglin, R. Carley, A. Castoldi, C. David, C. Deiter, F. Döring, R. Engel, F. Erdinger, H. Fangohr, C. Fiorini, P. Fischer, N. Gerasimova, R. Gort, F. deGroot, K. Hansen, S. Hauf, D. Hickin, M. Izquierdo, B. E. Van Kuiken, Y. Kvashnin, C.-H. Lambert, D. Lomidze, S. Maffessanti, L. Mercadier, G. Mercurio, P. S. Miedema, K. Ollefs, M. Pace, M. Porro, J. Rezvani, B. Rösner, N. Rothenbach, A. Samartsev, A. Scherz, J. Schlappa, C. Stamm, M. Teichmann, P. Thunström, M. Turcato, A. Yaroslavtsev, J. Zhu, M. Beye, H. Wende,

- U. Bovensiepen, O. Eriksson, A. Eschenlohr, The interplay of local electron correlations and ultrafast spin dynamics in fcc Ni. *Materials Research Letters* **11**, 655–661 (2023).
19. H. Öström, H. Öberg, H. Xin, J. LaRue, M. Beye, M. Dell'Angela, J. Gladh, M. L. Ng, J. A. Sellberg, S. Kaya, G. Mercurio, D. Nordlund, M. Hantschmann, F. Hieke, D. Kühn, W. F. Schlotter, G. L. Dakovski, J. J. Turner, M. P. Minitti, A. Mitra, S. P. Moeller, A. Föhlisch, M. Wolf, W. Wurth, M. Persson, J. K. Nørskov, F. Abild-Pedersen, H. Ogasawara, L. G. M. Pettersson, A. Nilsson, Probing the transition state region in catalytic CO oxidation on Ru. *Science* **347**, 978–982 (2015).
  20. K. S. Kumar, M. Ruben, Sublimable Spin-Crossover Complexes: From Spin-State Switching to Molecular Devices. *Angew. Chem. Int. Ed.* **60**, 7502–7521 (2021).
  21. M. Gruber, R. Berndt, Spin-Crossover Complexes in Direct Contact with Surfaces. *Magnetochemistry* **6**, 35 (2020).
  22. L. Kipgen, M. Bernien, F. Tuzcek, W. Kuch, Spin-Crossover Molecules on Surfaces: From Isolated Molecules to Ultrathin Films. *Adv. Mater.* **33**, 2008141 (2021).
  23. K. Ridier, A. Bas, V. Shalabaeva, W. Nicolazzi, L. Salmon, G. Molnár, A. Bousseksou, M. Lorenc, R. Bertoni, E. Collet, H. Cailleau, Finite Size Effects on the Switching Dynamics of Spin-Crossover Thin Films Photoexcited by a Femtosecond Laser Pulse. *Adv. Mater.* **31**, 1901361 (2019).
  24. R. Bertoni, M. Lorenc, A. Tissot, M.-L. Boillot, E. Collet, Femtosecond photoswitching dynamics and microsecond thermal conversion driven by laser heating in FeIII spin-crossover solids. *Coordination Chemistry Reviews* **282–283**, 66–76 (2015).
  25. M. Borchert, J. Braenzel, R. Gnewkow, L. Lunin, T. Sidiropoulos, J. Tümmeler, I. Will, T. Noll, O. Reichel, D. Rohloff, A. Erko, T. Krist, C. Von Korff Schmising, B. Pfau, S. Eisebitt, H. Stiel, D. Schick, Versatile tabletop setup for picosecond time-resolved resonant soft-x-ray scattering and spectroscopy. *Review of Scientific Instruments* **94**, 063102 (2023).
  26. M. Porro, L. Andricek, S. Aschauer, A. Castoldi, M. Donato, J. Engelke, F. Erdinger, C. Fiorini, P. Fischer, H. Graafsma, A. Grande, C. Guazzoni, K. Hansen, S. Hauf, P. Kalavakuru, H. Klaer, M. Tangl, A. Kugel, M. Kuster, P. Lechner, D. Lomidze, S. Maffessanti, M. Manghisoni, S. Nidhi, F. Okrent, V. Re, C. Reckleben, E. Riceputi, R. Richter, A. Samartsev, S. Schlee, J. Soldat, L. Struder, J. Szymanski, M. Turcato, G. Weidenspointner, C. B. Wunderer, The MiniSDD-Based 1-Mpixel Camera of the DSSC Project for the European XFEL. *IEEE Trans. Nucl. Sci.* **68**, 1334–1350 (2021).
  27. C. Cartier dit Moulin, P. Rudolf, A. M. Flank, C. T. Chen, Spin transition evidenced by soft X-ray absorption spectroscopy. *The Journal of Physical Chemistry* **96**, 6196–6198 (1992).
  28. J. Grunwald, J. Torres, A. Buchholz, C. Näther, L. Kämmerer, M. Gruber, S. Rohlf, S. Thakur, H. Wende, W. Plass, W. Kuch, F. Tuzcek, Defying the inverse energy gap law: a vacuum-evaporable Fe( II ) low-spin complex with a long-lived LIESST state. *Chem. Sci.* **14**, 7361–7380 (2023).



29. E. Stavitski, F. M. F. De Groot, The CTM4XAS program for EELS and XAS spectral shape analysis of transition metal L edges. *Micron* **41**, 687–694 (2010).
30. K. Zhang, G. S. Girolami, J. Vura-Weis, Improved charge transfer multiplet method to simulate *M*- and *L*-edge X-ray absorption spectra of metal-centered excited states. *J Synchrotron Rad* **25**, 1600–1608 (2018).
31. P. Dierks, A. Pöpcke, O. S. Bokareva, B. Altenburger, T. Reuter, K. Heinze, O. Kühn, S. Lochbrunner, M. Bauer, Ground- and Excited-State Properties of Iron(II) Complexes Linked to Organic Chromophores. *Inorg. Chem.* **59**, 14746–14761 (2020).
32. T. J. Penfold, E. Gindensperger, C. Daniel, C. M. Marian, Spin-Vibronic Mechanism for Intersystem Crossing. *Chem. Rev.* **118**, 6975–7025 (2018).
33. K. Bairagi, O. Iasco, A. Bellec, A. Kartsev, D. Li, J. Lagoute, C. Chacon, Y. Girard, S. Rousset, F. Miserque, Y. J. Dappe, A. Smogunov, C. Barreteau, M.-L. Boillot, T. Mallah, V. Repain, Molecular-scale dynamics of light-induced spin cross-over in a two-dimensional layer. *Nature Communications* **7**, 12212 (2016).
34. S. Johannsen, S. Ossinger, T. Markussen, F. Tuzcek, M. Gruber, R. Berndt, Electron-Induced Spin-Crossover in Self-Assembled Tetramers. *ACS Nano* **15**, 11770--11778 (2021).
35. W. Zhang, K. S. Kjær, R. Alonso-Mori, U. Bergmann, M. Chollet, L. A. Fredin, R. G. Hadt, R. W. Hartsock, T. Harlang, T. Kroll, K. Kubiček, H. T. Lemke, H. W. Liang, Y. Liu, M. M. Nielsen, P. Persson, J. S. Robinson, E. I. Solomon, Z. Sun, D. Sokaras, T. B. Van Driel, T.-C. Weng, D. Zhu, K. Wärnmark, V. Sundström, K. J. Gaffney, Manipulating charge transfer excited state relaxation and spin crossover in iron coordination complexes with ligand substitution. *Chem. Sci.* **8**, 515–523 (2017).
36. N. Gerasimova, D. La Civita, L. Samoylova, M. Vannoni, R. Villanueva, D. Hickin, R. Carley, R. Gort, B. E. Van Kuiken, P. Miedema, L. Le Guyarder, L. Mercadier, G. Mercurio, J. Schlappa, M. Teichman, A. Yaroslavtsev, H. Sinn, A. Scherz, The soft X-ray monochromator at the SASE3 beamline of the European XFEL: from design to operation. *J Synchrotron Rad* **29**, 1299–1308 (2022).
37. N. Rothenbach, M. E. Gruner, K. Ollefs, C. Schmitz-Antoniak, S. Salamon, P. Zhou, R. Li, M. Mo, S. Park, X. Shen, S. Weathersby, J. Yang, X. J. Wang, R. Pentcheva, H. Wende, U. Bovensiepen, K. Sokolowski-Tinten, A. Eschenlohr, Microscopic nonequilibrium energy transfer dynamics in a photoexcited metal/insulator heterostructure. *Phys. Rev. B* **100**, 174301 (2019).
38. F. Döring, B. Rösner, M. Langer, A. Kubec, A. Kleibert, J. Raabe, C. A. F. Vaz, M. Lebugle, C. David, Multifocus off-axis zone plates for x-ray free-electron laser experiments. *Optica* **7**, 1007 (2020).
39. V. Blum, R. Gehrke, F. Hanke, P. Havu, V. Havu, X. Ren, K. Reuter, M. Scheffler, Ab initio molecular simulations with numeric atom-centered orbitals. *Computer Physics Communications* **180**, 2175–2196 (2009).
40. J. Heyd, G. E. Scuseria, M. Ernzerhof, Hybrid functionals based on a screened Coulomb potential. *The Journal of Chemical Physics* **118**, 8207–8215 (2003).

41. M. Reiher, O. Salomon, B. Artur Hess, Reparameterization of hybrid functionals based on energy differences of states of different multiplicity. *Theoretical Chemistry Accounts: Theory, Computation, and Modeling (Theoretica Chimica Acta)* **107**, 48–55 (2001).
42. O. Salomon, M. Reiher, B. A. Hess, Assertion and validation of the performance of the B3LYP\* functional for the first transition metal row and the G2 test set. *The Journal of Chemical Physics* **117**, 4729–4737 (2002).
43. L. Lehtovaara, V. Havu, M. Puska, All-electron density functional theory and time-dependent density functional theory with high-order finite elements. *The Journal of Chemical Physics* **131**, 054103 (2009).
44. C. M. Marian, Spin-orbit coupling and intersystem crossing in molecules: Spin-orbit coupling. *WIREs Comput Mol Sci* **2**, 187–203 (2012).
45. A. Hauser, “Light-Induced Spin Crossover and the High-Spin→Low-Spin Relaxation” in *Spin Crossover in Transition Metal Compounds II* (Springer Berlin Heidelberg, Berlin, Heidelberg, 2004; <http://link.springer.com/10.1007/b95416>) vol. 234 of *Topics in Current Chemistry*, pp. 155–198.

### Acknowledgments

We acknowledge European XFEL in Schenefeld, Germany, for provision of x-ray free electron laser beamtime at Scientific Instrument Spectroscopy and Coherent Scattering and would like to thank their staff for the excellent assistance before, during, and after the beamtime. We thank Thies J. Albert, Jennifer Schmeink, Samuel Palato, Sergey Kovalenko, and Julia Stähler for supporting measurements as well as Christel Marian, Eberhard K. U. Gross and Georg Jansen for fruitful discussions.

### Funding:

German Research Foundation Project-ID 278162697 – SFB 1242, projects A05, A07, A08, B02, and C01

German Research Foundation grant INST 20876/209-1 FUGG

German Research Foundation grant INST 20876/243-1 FUGG

German Research Foundation grant TU58/18-1

## Figures and Tables

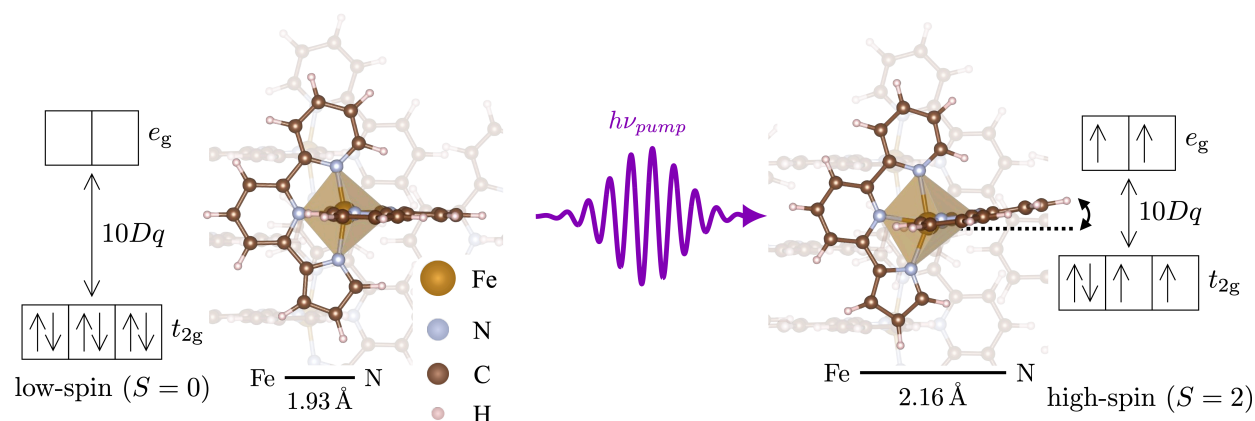


**Fig. 1. Low- and high-spin configurations in spin-crossover molecules.** The calculated geometries of an individual [Fe(pypypyr)<sub>2</sub>] molecule in the low-spin ( $S = 0$ , left) and high-spin ( $S = 2$ , right) state. Concomitantly with the low- to high-spin transition, the Fe-N bond length changes by approximately 10% as indicated by the corresponding averaged bond lengths inferred from DFT calculations. The corresponding ligand twisting in the high-spin state is indicated on the right by the dashed line and the bended arrow. The excitation of the molecule by an external stimulus, such as a pump laser pulse at photon energy  $h\nu_{pump}$ , can trigger this transition. The splitting of  $3d$  states of the Fe ion into  $t_{2g}$  and  $e_g$  in an octahedral ligand field is represented by the  $10Dq$  value as indicated at the left and right side for  $S = 0$  and  $S = 2$ , respectively. In the condensed form, the molecules are surrounded by peers, as illustrated with molecules in light colors in the background, which can further modify the switching properties.

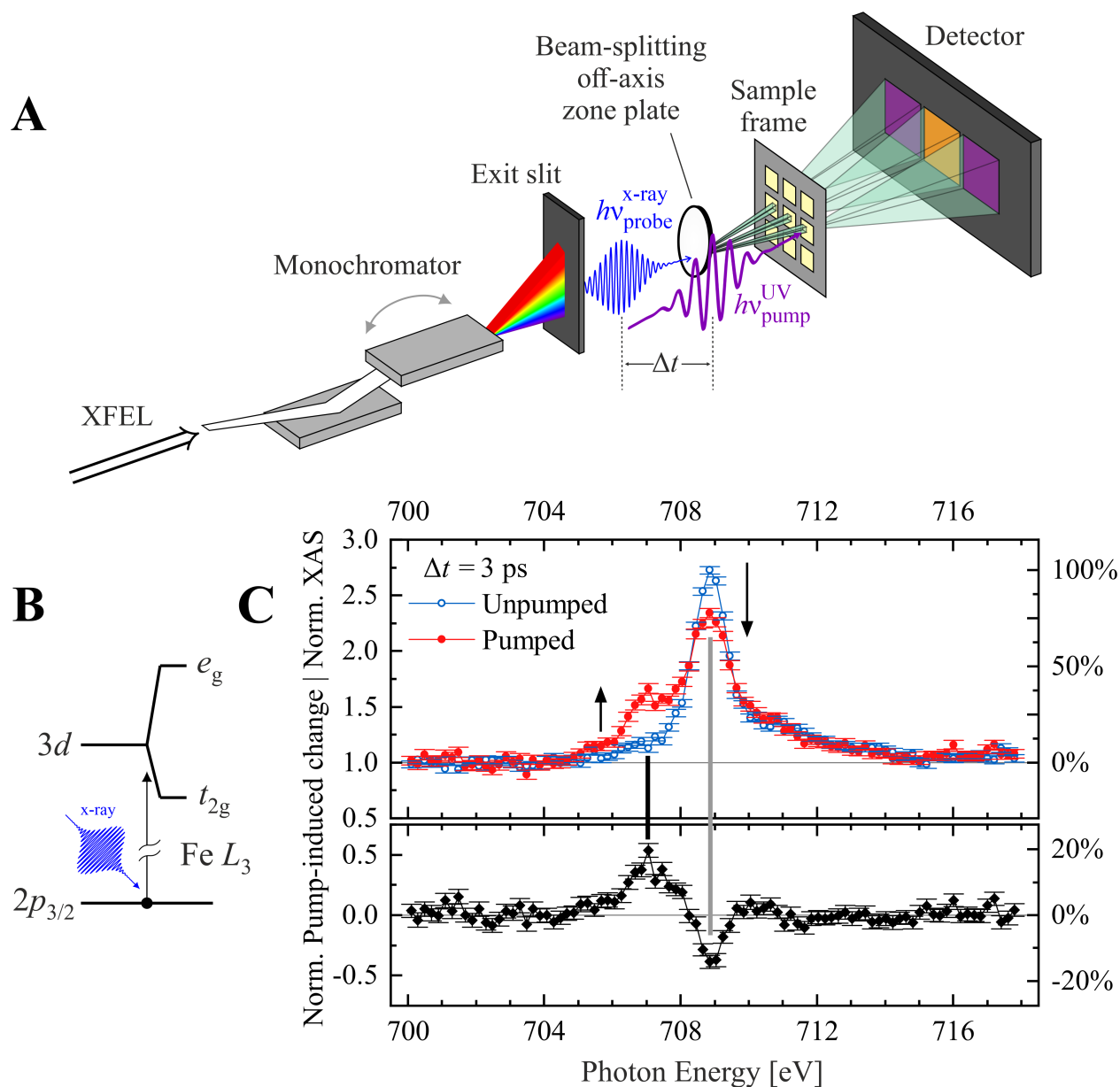


**Fig. 2. Time-resolved x-ray absorption spectroscopy at the Fe  $L_3$  edge.** (A) Experimental setup of the Spectroscopy and Coherent Scattering Instrument at the European XFEL. The SASE3 undulator system generates x-ray pulses, which are monochromatized by a variable line-spacing grating in combination with an exit slit. The x-rays then pass through beam-splitting off-axis zone plate optics which split the x-ray beam into three beams of equal intensity. These beams are transmitted through the sample structure consisting of one bare  $\text{Si}_3\text{Ni}_4$  membrane and two molecular films on such membranes, one of them is pumped. The three beams are detected on an imaging detector (26) to distinguish the three signals. This setup allows for pulse to pulse normalization, which is essential for a fluctuating light source as used here, see (17) for details. (B) Schematic x-ray absorption process for the measured fine structure at the Fe  $L_3$  absorption edge. The x-ray pulses excite electrons resonantly from the  $2p_{3/2}$  state to unoccupied  $3d$  states. Due to the splitting of the  $3d$  state into a  $t_{2g}$  and an  $e_g$  state, x-ray spectroscopy is sensitive to low- and high-spin states of the spin-crossover molecule. (C) An x-ray absorption spectrum of the molecular film measured at room temperature at the unpumped window (open circles, blue) is depicted together with a pumped spectrum (filled circles, red) at time delay  $\Delta t = 3$  ps, which was recorded at a laser pumped membrane window. Both spectra

are corrected with the simultaneously measured  $I_0$  on a reference  $\text{Si}_3\text{N}_4$  window. Details on the normalization are given in the supplementary materials. The difference of the pumped and the unpumped spectrum represents the pump-induced change (bottom panel). The right axis is given relative to the maximum of the unpumped spectrum. The two features in the spectrum at photon energies of 707.1 eV and 708.9 eV, see vertical lines, show changes in intensities that are highlighted by arrows. This spectral modification is represented by the pump-induced change and corresponds to the spin-state switching from  $S = 0$  to  $S = 2$ , induced by the pump laser at an incident fluence of  $10 \text{ mJ/cm}^2$ .

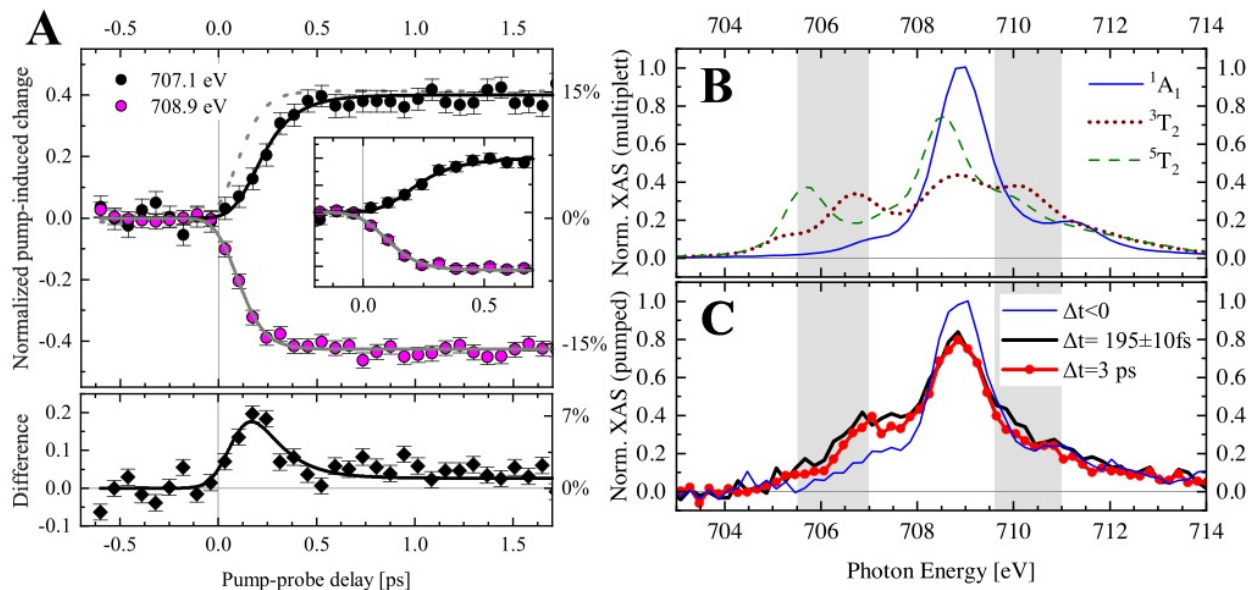


**Fig. 3. Intermediate state analysis of the spin-crossover process.** (A) Top panel: Normalized pump-induced change at 707.1 eV (black symbols) and 708.9 eV (pink symbols) photon energy as a function of pump-probe delay  $\Delta t$ . The lines guide the eye. The gray dashed line is the absolute value of the guide to the eye of the negative transient for 708.9 eV. The right ordinate indicates the ratio to the maximum in the unpumped spectrum, see Fig. 2C. Inset: The data of the main panel are presented for a reduced time delay range. Bottom panel: The difference of the two transient absorption traces shown in the top panel are depicted. (B) Multiplet calculations for x-ray absorption spectra calculated using CTM4XAS (29) in combination with scripts from Zhang et al. (30) for the fixed low spin nuclear geometry and varying the total spin  $S=0$  ( $^1A_1$ , blue),  $S=1$  ( $^3T_2$ , brown, dotted),  $S=2$  ( $^5T_2$ , green, dashed). (C) x-ray absorption spectra at three different time delays  $\Delta t$ : before pumping (blue), at 195 fs (black), and at 3 ps (red) normalized to the white line intensity at 708.9 eV. In the region of the gray bar the spectrum at 195 fs exhibits absorption at lower energy than the one at 3 ps. The spectra are normalized to their peak maximum of the corresponding unpumped spectra.

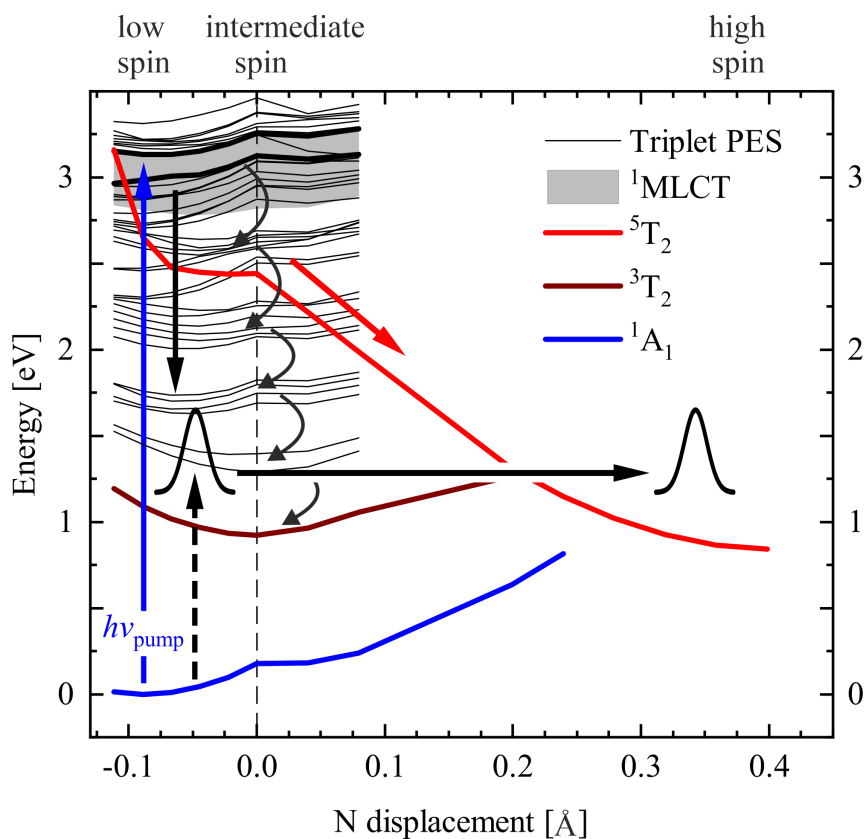


**Fig. 4. Calculated potential energy surfaces.** Total energies of the metal-centered  $S = 0$  ( $^1A_1$ ),  $S = 1$  ( $^3T_2$ ), and  $S = 2$  ( $^5T_2$ ) (thick lines) states, as well as  $^1MLCT$  singlet (gray area), and metal-ligand triplet states (thin lines) as a function of the N displacement as inferred from TD-DFT; see the main text, also for discussion of the arrows. The vertical dashed arrow is an Auger-like excitation from  $^1A_1$  to  $^3T_2$  in response to the electronic relaxation out of the  $^1MLCT$  state. The N displacement is changed along two coordinates to represent the low-, intermediate-, and high-spin states. The transition from the intermediate- to the low- or to the high-spin state not only includes a change of the Fe-N bond length, but also a distortion of the octahedral geometry.

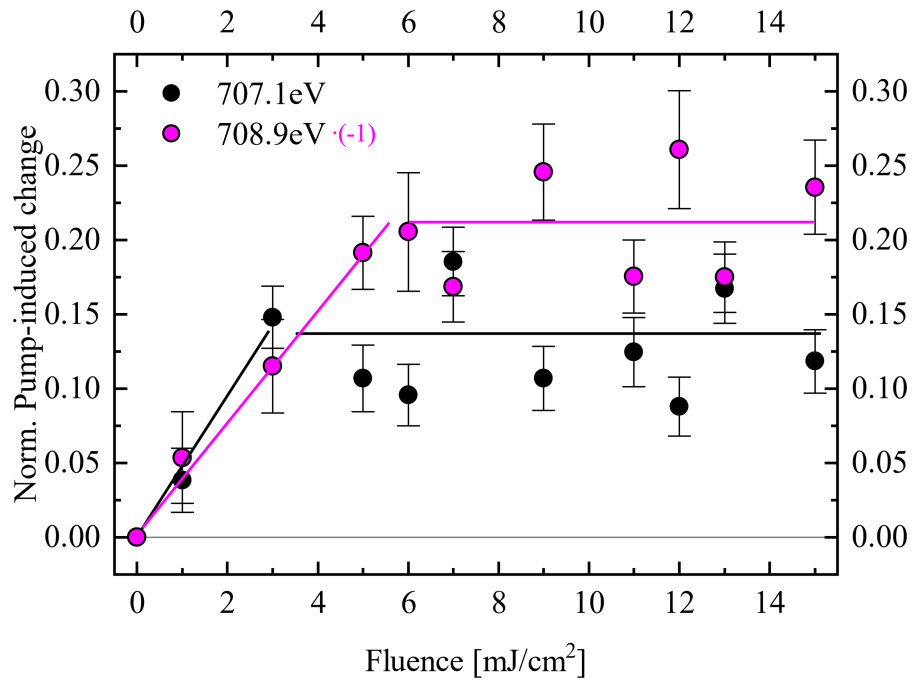


**Fig. 5. Pump fluence dependence of the pump-induced change.** The normalized pump-induced change at 3 ps time delay is plotted as a function of incident pump fluence in the x-ray absorption at the two features in the fine structure as indicated by the given photon energy. For clarity, the absolute value of the negative pump-induced change at 708.9 eV photon energy is depicted. The considerable fluctuations of the pump-induced changes are assigned to modifications in spatial overlap of pump and probe pulse upon varying the fluence. Within the available data quality, we identify an increase in the pump-induced change to about 5 mJ/cm<sup>2</sup> and a saturation of these signals for larger pump fluence.

## Supplementary Text

### Sample preparation

The Fe(II) spin-crossover complex [Fe(pypypyr)<sub>2</sub>] was synthesized as described in (28). An (20 × 20) array of 100 nm thick Si<sub>3</sub>N<sub>4</sub> windows were used as substrates. The molecular films were prepared at a pressure  $p = 6.3 \cdot 10^{-8}$  mbar, which is determined by the vapor pressure of the complex at the sublimation temperature of 534 K. The evaporation rate was measured before and after deposition using a quartz balance turned to the same position as the sample for evaporation. Ultrathin molecular films on Si<sub>3</sub>N<sub>4</sub> were obtained by sublimating under these conditions for 34 min. Before evaporation, every third column was covered. The corresponding windows, free of molecules, are used for normalization to consider variations in the x-ray fluence. Fig. S1 shows a typical sample with a pattern of covered and uncovered columns.

### Time-resolved x-ray absorption spectroscopy measurement setup

The measurements were performed at the Spectroscopy and Coherent Scattering (SCS) instrument of European XFEL using a pump-probe setup with an effective time resolution of 70-80 fs (17), estimated from the pulse duration of the optical laser (50 fs) and the FEL (30-60 fs) as well as taking the relative arrival time jitter (15 fs) into account. The energy resolution of the monochromator is 200 meV (36). The European XFEL provides a pulse pattern of subsequent pulse trains with a train repetition rate of 10 Hz. If not specified otherwise, the measurements were performed with a pulse train consisting of 9 x-ray pulses with an intra-train repetition rate of 22.5 kHz, i.e., the x-ray pulses are 44 μs apart in a train.

The optical laser arrival time, time zero  $t_0$ , was determined by measuring the pump-induced change of a reference 16 nm Fe film capped with 2 nm MgO on Si<sub>3</sub>N<sub>4</sub> membranes. For this experiment, one train consisted of 50 pulses with an intra-train repetition rate of 226 kHz. The film exhibited a steep pump-induced change at the Fe  $L_3$  edge consistent with previous findings (37).

### Determination of time-resolved x-ray absorption spectra

Because of the intensity fluctuations of the x-ray pulses in the self-amplified spontaneous emission (SASE) process at an XFEL, the x-ray absorption spectra (XAS) are measured in transmission geometry with the beam-splitting off-axis zone plate setup (17, 38). The spectra are evaluated with the Spectroscopy and Coherent Scattering (SCS) Instrument toolbox (17) utilizing the flat-field and non-linearity corrections. The x-ray absorption spectra are calculated by taking the negative logarithm of the transmitted signal divided by the reference signal of the bare substrate. The pump-induced change is calculated from the negative logarithm of the fraction of the XAS spectrum for the sample irradiated by the optical pump-laser (pumped spectrum) and the XAS spectrum measured in parallel at a neighboring sample without the optical pump (unpumped spectrum). For these measurements it is essential that the two samples prepared on the Si<sub>3</sub>N<sub>4</sub> windows are as identical as possible, e.g., with respect to the molecular film thickness. Our investigations show that this analysis is possible using molecular films prepared by sublimation.

The pumped and unpumped spectra exhibit different offset backgrounds potentially originating from the off-axis zone plate. To correct for this effect, we measured Si<sub>3</sub>N<sub>4</sub> references in which three adjacent membrane windows were left blank to obtain a direct correction for each window and the detector frame. However, an offset and slight linear background still exist and are corrected using two linear functions, one for the pre-edge regime and one for the post-edge regime. These two functions are then utilized to derive an overall linear function that characterizes the spectrum's background.



We measured the absorption of x-ray pulses at a given energy, from which the average and standard deviation are calculated. In cases where spectra are averaged, the error is calculated via error propagation of the standard errors of the individual spectra. After correcting the background, the spectra shown in Fig. 2 were normalized so that the mean of the pre-edge region equals one. Similarly, the spectra in Fig. 3 were normalized to coincide with a peak intensity equal to one at the maximum of the white line (708.9 eV). The spectra displayed in Figures 2 and 3C ( $\Delta t < 0$ ,  $\Delta t = 3$  ps) are averaged over 3 to 4 sweeps.

The fluctuations in the time  $t_0$  are on the order of  $\pm 10$  fs per hour. To minimize the impact of the time drift, we acquired the pump-induced changes measured at fixed x-ray photon energies with varying delay of the optical pump  $\Delta t$  (delay scans, Fig. 3A) in an alternating manner. First, the time-delay scan at 707.1 eV was measured for 20 min, followed by the scan at 708.9 eV, then back at 707.1 eV and so on. For each pair of scans, the scan at 708.9 eV is fitted with

$$\Theta(x - t_0) \cdot \left( A_1 \cdot \left( 1 - e^{-(x-t_0)/t_1} \right) \right)$$

time zero  $t_0$ , the time constant  $t_1$ , and the amplitude  $A_1$ . The pairs of scans were then corrected for their variations in  $t_0$  before averaging. To normalize the amplitude of the delay scans, the x-ray absorption measured at  $\Delta t = 1$  ps was used.

#### Pumped XAS spectra in the femtosecond time regime

Figure 3C in the main manuscript shows pumped XAS spectra in the femtosecond (fs) time regime. The 195 fs spectrum is the average over three spectra. Because of the drift of  $t_0$ , these three spectra correspond to slightly different delays: 184, 197, and 204 fs. For completeness, the individual spectra as well as the average are shown in Figure S3.

#### Optical Microscopy

Optical microscopy images were taken using a Keyence VHX-6000 digital microscope. These measurements were performed to verify the mounting and layout of all samples. An example image of a  $\text{Si}_3\text{N}_4$  frame is shown in Fig. S1.

#### UV-Vis spectroscopy

The UV/Vis spectra were recorded with a Cary 5000 spectrometer (Varian) in transmission geometry. Solutions of different concentrations were prepared by dissolving 61, 95, 200, 306, and 493  $\mu\text{g}$  (uncertainty of  $\pm 1$   $\mu\text{g}$ ) in 10 mL of absolute dichloromethane in a volumetric flask. A double beam setup was used, measuring the absorbance of the solution relative to that of the pure solvent. The corresponding UV-Vis spectra are shown in Fig. S2B. Several absorption bands are observed, including one centered at a wavelength of 430 nm. The optical excitation for the time-resolved XAS measurements at a wavelength of 400 nm (or 3.1 eV photon energy) is done at the edge of this charge-transfer absorption band.

From the evolution of the absorbance with the concentration, a molar absorption coefficient of  $1 \cdot 10^3 \text{ m}^2 \text{ mol}^{-1}$  at 400 nm is extracted, which corresponds to an absorption cross-section of  $\sigma = 3.82 \cdot 10^{-17} \text{ cm}^2$ . Owing to the low photon absorption, we conclude that the photon density is homogeneous across the molecular film. The absorbed energy (per  $\text{cm}^2$ ) is therefore given by

$$-\Delta\Phi = \Phi_0 n \sigma d$$

where  $\Phi_0$  is the incident photon fluence,  $n$  the density of molecules,  $d$  the thickness of the film, and  $\Delta\Phi$  the variation of the fluence across the film. The fraction of molecules absorbing a photon reads:

$$\frac{-\Delta\Phi}{n d h \nu} = \frac{\Phi_0 \sigma}{h \nu}$$

where  $h \nu$  is the photon energy of 3.1 eV of the pump pulse. With  $\Phi_0 = 13 \text{mJ} \cdot \text{cm}^{-2}$ , every molecule absorb a photon.

### Density Functional Theory

The atomic and electronic structure of single molecules was studied by density functional theory using the FHI-aims code (39). The hybrid functional HSE06 (40) was used to describe the electronic exchange and correlation, with the admixture of exact exchange reduced to  $\alpha=10\%$ . This value was chosen to reproduce the optical absorption spectrum of the molecule as obtained from the LR-TDDFT calculations (see Fig. S2A and further details below). Our finding that a reduced  $\alpha$  provides a better description of the Fe complex is consistent with previous observations that Fe coordination complexes are best described by such a reduced  $\alpha$  parameter (41, 42). The FHI-Aims code is an all-electron electronic structure code that uses numerically defined atom-centered orbitals. The so-called "tight" settings for the basis set and real-space sampling were used to optimize the atomic structure of the molecule using the forces obtained from DFT.

The scalar-relativistic calculations were performed in three different spin states,  $S = 0, 1, 2$ . For  $S = 1$  and  $S = 2$ , the spin-up and spin-down Kohn-Sham orbitals are described by separate wave functions. The total magnetic moment of the molecules was constrained to optimize the geometries in each specific spin state.

While the rearrangement of atomic positions associated with a change in spin state occurs in a multidimensional configuration space, for clarity we have chosen a simplified reaction pathway consisting of two segments. We connect the optimized  $S = 1$  geometry to both the  $S = 2$  geometry (positive reaction coordinate) and the  $S = 0$  geometry (negative reaction coordinate) by linear interpolation of all atomic coordinates in the multidimensional configuration space. The average displacement of all six nitrogen atoms was used as a quantitative measure of the reaction coordinate. The total energies obtained along these linear segments are represented by the thick curves in Fig. 3B.

To study the electronic excitations of the molecule as a whole, we use the linear response formalism within time-dependent density functional theory (TDDFT) as implemented in the FHI-aims code (39). The excitation energies for singlet and triplet excitations were obtained by solving the Casida equation (43). The wave functions of the  $S=0$  state along the reaction path, increased by unoccupied orbitals, served as a starting point. The triplet potential energy surfaces (light curves in Fig. 3B) were obtained by adding the triplet excitation energies to the total energy of the  $S=0$  ground state. In addition, the optical absorption spectrum was calculated using the singlet excitation energies and the oscillator strengths obtained from the Casida equation (Fig. S2A) and compared to the experimental spectrum in Fig. S2B. The absorption peaks at 640 nm and 420 nm, in addition to the strong absorption below 370 nm, were reproduced by the calculation, indicating that the choice of the density functional is appropriate.

The results show that the Fe complex, including its organic ligands, exhibits a variety of electronic excitations, both singlets and triplets. In particular, there are a large number of  $^1\text{MLCT}$  states in the energy range of about 3 eV above the ground state, which corresponds to the energy of the light used to optically pump the molecule. Therefore, it is highly plausible that the optical excitation initially populated an MLCT singlet state. Our calculations

(neglecting spin-orbit coupling) show numerous crossings between excited singlet and triplet states, see Fig. 3B. This allows for an efficient spin state change from  $S = 0$  to  $S = 1$  when spin-orbit coupling is considered, as shown previously (44). Similarly, we expect that the inclusion of spin-orbit coupling will lead to transitions between the numerous  $S = 1$  states and the  $S = 2$  potential energy curve at positive values of the reaction coordinate. According to previous theoretical studies (13), the associated time scales for these inter-system crossings are less than 100 fs.

Given the theoretical results, the intermediate state derived from the experimentally observed dynamics should be understood as a molecule that is (for a very short time) in one of the many possible triplet states. We note that the multitude of triplet states found for this particular tridentate complex with organic ligands, each consisting of three organic rings, allows electronic relaxation by Auger-like processes, i.e., a high-lying triplet (or singlet) can decay into two lower-lying triplets. Such an electronic relaxation pathway could well compete with an alternative relaxation mechanism in which the excitation energy is distributed among the vibrational modes of the molecule.

To investigate the dependence of atomic motion and inertia associated with the atomic masses in the dynamics, we performed a classical molecular dynamics simulation on the  $S = 2$  potential energy surface. The simulation was performed at zero temperature using the geometry optimized for the  $S = 1$  configuration as a starting point. Again, the HSE06 functional with  $\alpha = 10\%$  is used to calculate the total energy. It can be seen that the atomic configuration moves towards the  $S = 2$  energy minimum within  $t = 70$  fs. Thus, combining the knowledge of fast intersystem crossing with the information obtained from the molecular dynamics simulation, the theory supports the spin switching with 200 fs observed in the experiment.

### Multiplet calculations

The XAS at the Fe  $L_3$  edge were simulated using the CTM4XAS software (29) (Version 5.5) in combination with the scripts from Zhang (30) allowing the computation of multiplets of excited states. All the spectra were computed assuming an octahedral ligand field with  $10 Dq = 2.6$  eV, as suggested by our DFT calculations for the low-spin state. The Slater integral parameters were kept to their default values (80 % of the Hartree-Fock values), the spin-orbit constants are unmodified, and no charge transfer was considered. The plotted spectra correspond to Gaussian ( $\sigma_G = 0.25$  eV) and Lorentzian ( $\sigma_L \approx 0.2$  eV) broadened calculated transitions.

### Three state model

The time-dependent experimental data can be reproduced by considering three states: the low-spin (LS), the high-spin (HS), and an intermediate (IS) spin state. The populations of these states are inferred from a rate equation model:

$$p_{LS}(t) = e^{-k_{LS \rightarrow IS} t}$$

$$p_{IS}(t) = \frac{k_{LS \rightarrow IS}}{k_{IS \rightarrow HS} - k_{LS \rightarrow IS}} (e^{-k_{LS \rightarrow IS} t} - e^{-k_{IS \rightarrow HS} t})$$

$$p_{HS}(t) = 1 - \frac{k_{LS \rightarrow IS}}{k_{IS \rightarrow HS} - k_{LS \rightarrow IS}} \left( \frac{k_{IS \rightarrow HS}}{k_{LS \rightarrow IS}} e^{-k_{LS \rightarrow IS} t} - e^{-k_{IS \rightarrow HS} t} \right),$$

with  $k_{LS \rightarrow IS}$  ( $k_{IS \rightarrow HS}$ ) the transition rate from the LS to the IS (IS to the HS) state. The HS to LS relaxation rate is on the order of  $10^9$  s<sup>-1</sup> for LS compounds at RT (45), i.e., four orders of

magnitude lower than the other rates, and is therefore neglected here. The x-ray absorption (XA) at a given photon energy  $h\nu$  is then given by

$$XA^{h\nu}(t) = p_{LS} \cdot XA_{LS}^{h\nu} + p_{IS} \cdot XA_{IS}^{h\nu} + p_{HS} \cdot XA_{HS}^{h\nu},$$

where  $XA_i^{h\nu}$  is the x-ray absorption of state  $i$  at the photon energy  $h\nu$  (see Fig. S4).

The difference in absorption (between the pumped and unpumped windows) is  $\Delta XA^{h\nu}(t) = XA^{h\nu} - XA_{LS}^{h\nu}$ . To account for the limited time resolution of the instrumentation,  $\Delta XA^{h\nu}(t)$  is convolved with

$$G(t) = \frac{1}{\sigma^2 \sqrt{2\pi}} \exp\left(-\frac{t^2}{2\sigma^2}\right),$$

where  $\sigma$  is related to the time resolution of the instrument (here  $\tau_{Res} = 2\sqrt{2 \ln 2} \cdot \sigma \approx 80$  fs). The experimental delay scans can be reproduced with  $\Delta XA^{h\nu} * G$  using

$$XA_{IS}^{707.1} \approx 0.08, XA_{IS}^{708.9} \approx 0.33, k_{LS \rightarrow IS} = 8.3 \times 10^{12} \text{ s}^{-1}, \text{ and } k_{IS \rightarrow HS} = 7.4 \times 10^{12} \text{ s}^{-1}.$$

The corresponding time constants are  $\tau_{LS \rightarrow IS} = 120$  fs and  $\tau_{IS \rightarrow HS} = 135$  fs. It should be noted that given the uncertainty of the real spectral line shape of the intermediate state, the uncertainty on the time zero and considering the time resolution of the instrument, the time constants given here should be taken with care. However, the model shows that the experimental data are compatible with a  ${}^3T_2$  intermediate state.

The inset in Fig. S4B shows the evolution of the spin-state populations as a function of the time inferred from Eq. 5 and using rates compatible with the experimental data. It should be noted that the red spectrum in Fig. S4A. is not that of a pure HS but contains approximately 60 % of LS molecules. We consider an intermediate-state spectrum composed of 40 % of molecules in  ${}^3T_2$  and 60 % in the LS state.  $p_{LS}$ ,  $p_{IS}$ , and  $p_{HS}$  therefore describe the populations of switchable molecules.

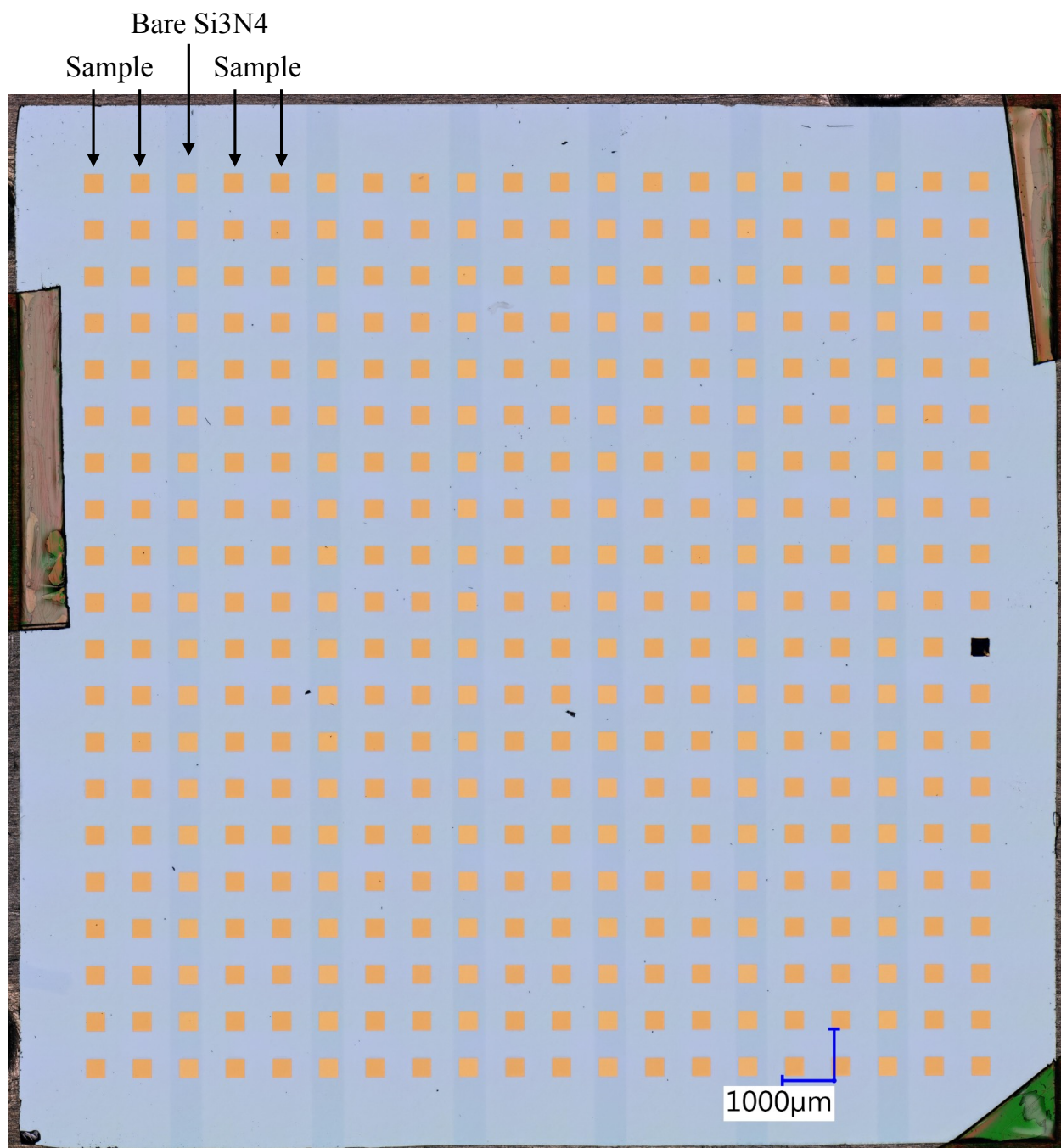


**Fig. S1.**

Optical microscope image of a sample frame with  $[\text{Fe}(\text{pypypyr})_2]$  on  $\text{Si}_3\text{N}_4$  in combination with bare  $\text{Si}_3\text{N}_4$  as indicated on the top left, recorded with a Keyence VHX-6000 digital microscope. The variations of color indicate the columns that were covered during the evaporation process to keep these particular  $\text{Si}_3\text{N}_4$  windows bare (used for reference signal). The darker window on the right side is broken.

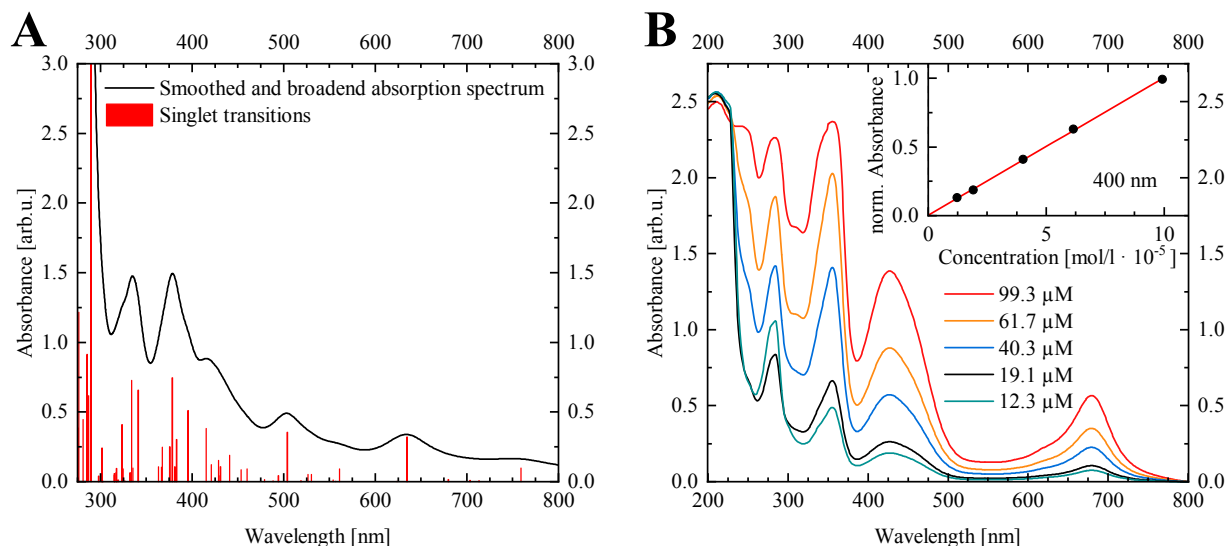


**Fig. S2.**

**(A)** Optical absorption of  $[\text{Fe}(\text{pypypyr})_2]$  as obtained from linear-response TDDFT calculations using the HSE06 hybrid functional with  $\alpha$  reduced to 10%. The red bars indicate the oscillator strength of the singlet transitions. The black line is an absorption spectrum obtained by smoothing with a Lorentzian line width of 0.1 eV. The long-wavelength transitions at  $\lambda=640$  nm and 760 nm are Laporte-forbidden transitions between occupied and unoccupied Fe  $3d$  orbitals. The transitions around 400 nm are metal-to-ligand transitions into unoccupied states of the organic ligands. These are used for optically pumping the molecular spin switching. **(B)** UV-Vis spectra of different concentrations as indicated dissolved in dichloromethane. The inset shows the absorption at 400 nm wave length used in the optical pumping as a function of the concentration of the solution.

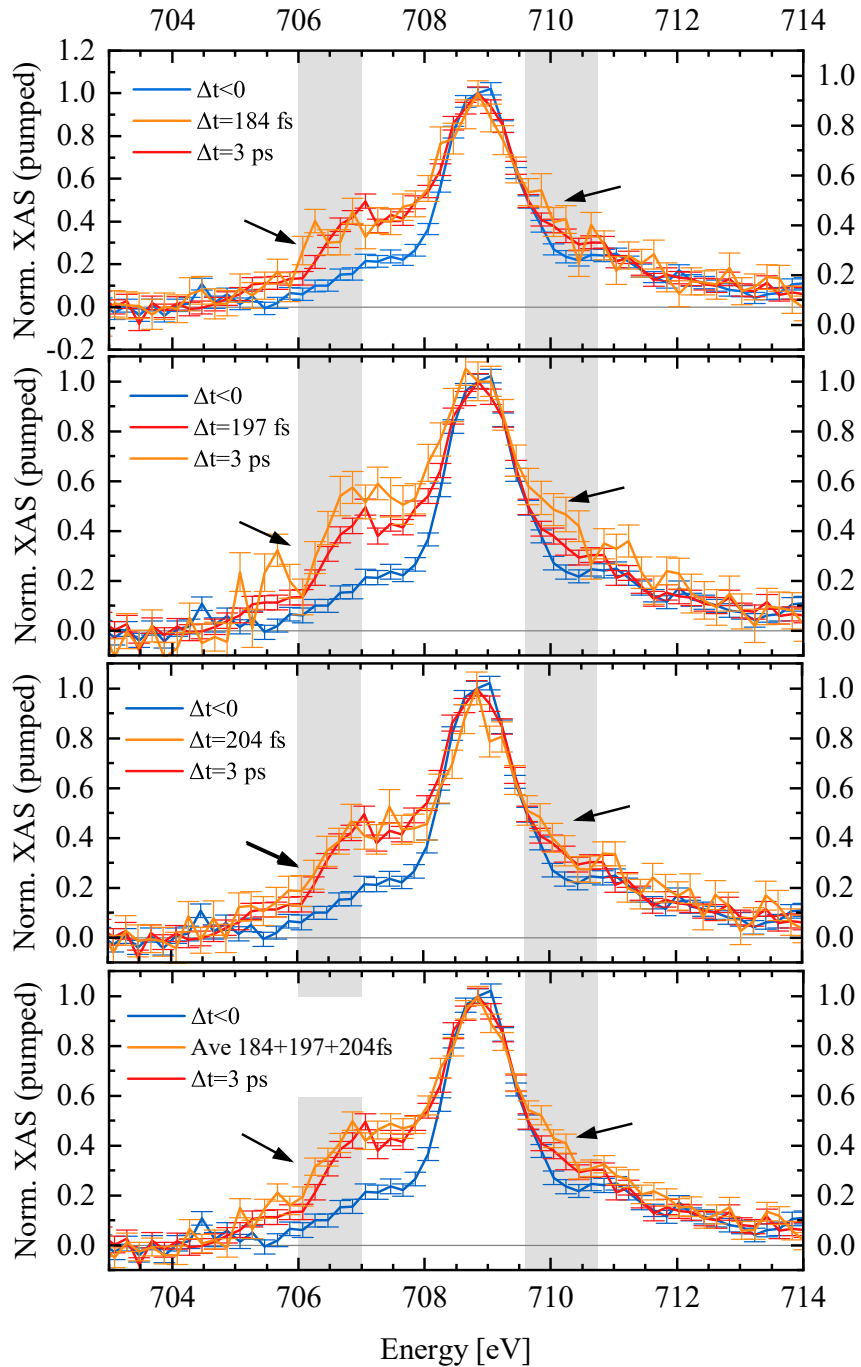


**Fig. S3.**

Experimental x-ray absorption spectra at three different time delays (orange):  $\Delta t = 184$  fs, 197 fs, 204 fs, and the average of the three from the top to the bottom, respectively. The latter is shown in the main manuscript as Fig. 3C. The spectra for  $\Delta t < 0$  (blue) and  $\Delta t = 3$  ps (red) were used as references for the initial and final states visible in the spectra in all three panels. Normalization was done to the white line intensity at 708.9 eV for all spectra. The arrows indicate regions (grey areas) of added absorption in comparison to the blue ( $\Delta t < 0$ ) and red ( $\Delta t = 3$  ps) spectra.

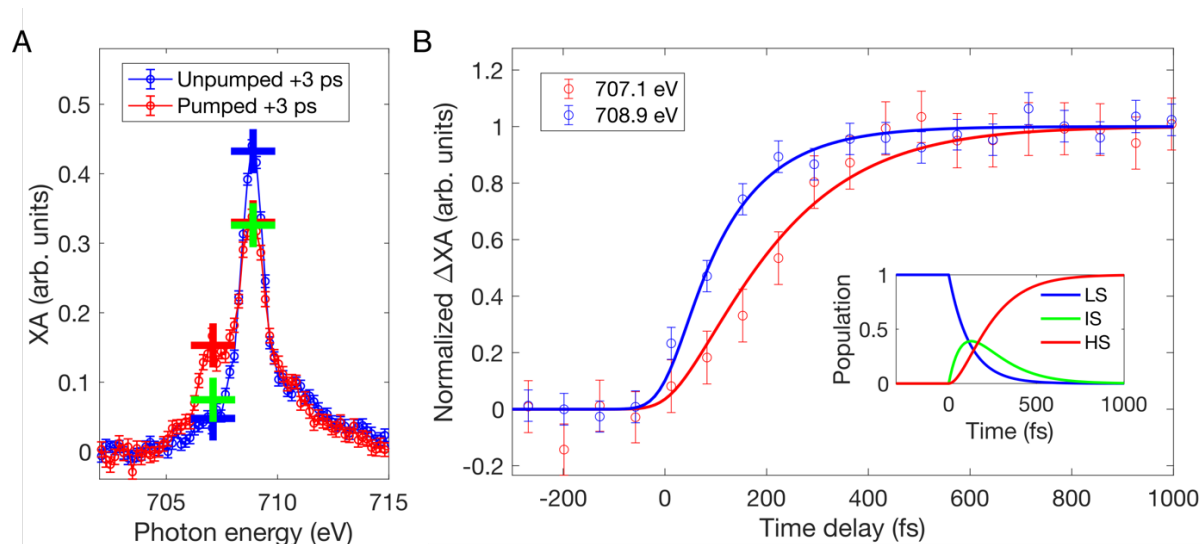


**Fig. S4.**

**(A)** XAS of the pumped (red) and unpumped (blue) SCO film on  $\text{Si}_3\text{N}_4$ . The crosses indicate the XA of the LS (blue), IS (green) and HS (red) states at 707.1 and 708.9 eV used for the model. The XA of the IS state is based on 40 % of the multiplet calculations of the  ${}^3T_2$  state in the LS geometry ( $10 Dq = 2.6$  eV) along with 60 % of LS molecules. **(B)** Experimental delay scans at photon energies of 707.1 eV (red circles) and 708.9 eV (blue circles). The solid lines correspond to  $\Delta XA^{h\nu} * G$  of the three-state model described in the text assuming  $\tau_{\text{LS} \rightarrow \text{IS}} = 120$  fs,  $\tau_{\text{IS} \rightarrow \text{HS}} = 135$  fs, and a time resolution of 80 fs for the instrument. Note that the amplitudes have been manually scaled. The  $t_0$  of the data has been shifted by 20 fs. The inset shows the corresponding populations of the LS, IS, and HS states as a function of time.